

Turbulent flux over land and sea as a Kelvin wave propagates through different phases of the MJO

Crizzia Mielle De Castro

Abstract

The MJO modulates extratropical waves, which can trigger Kelvin waves as they break into the tropics. Consequently, equatorial Kelvin waves can influence the evolution and timing of extratropical waves and new MJO events. This necessitates investigating Kelvin waves and the MJO propagating together and their effects on the tropical atmosphere. This study investigates the evolution of vertical turbulent flux of momentum, heat, and moisture within the boundary layer as a Kelvin wave propagates along the Indian ocean and Maritime Continent during the different phases of the MJO. 2-dimensional Fourier filtering applied to OLR differentiated Kelvin waves from other convectively-coupled equatorial waves. Regression was also used to remove the seasonal cycle and calculate the anomalies of vertical and zonal wind, air temperature, and specific humidity, which were used to calculate the vertical turbulent flux. This study found that momentum flux tends to be more positive over water than over land. Furthermore, the heat flux tends to be more positive during the MJO's suppressed convective phase over water and enhanced convective phase over land. The inversion of heat flux also occurs at a higher altitude over water than over land. Lastly, the moisture flux tends to increase faster with height during the MJO's enhanced convective phase over water, but inverts at around 500 m over land.

1 Introduction

1.1 Background on Kelvin waves and the MJO

Convectively-coupled equatorial waves influence rainfall, wind patterns, and tropical cyclone formation across the tropics [1]. Of interest in this study are equatorial Kelvin waves, synoptic scale eastward moving convective disturbances with phase speeds of $9 - 20 \text{ m/s}$ [2].

The fast-moving Kelvin waves comprise a slower-moving planetary scale convective structure known as the Madden-Julian oscillation (MJO) [3]. The MJO propagates eastward as well at phase speeds of $4 - 8 \text{ m/s}$ [4]. Wheeler and Hendon (2004) [5] developed a real-time multivariate MJO (RMM) index that describes the longitudinal location of the MJO as it propagates eastward (illustrated in Fig. 1). For example, at RMM phase seven, the MJO's suppressed convection occurs over the Indian ocean, and the MJO's enhanced convection occurs over the west Pacific ocean.

Despite the physical distinction between the two, the MJO modulates Rossby gyres [6], which can trigger Kelvin waves as they break into the tropics [7]. Consequently, equatorial Kelvin waves can influence the evolution and timing of extratropical waves and new MJO events. This necessitates investigating Kelvin waves and the MJO together and not just as separate entities. The alternating patterns of wind shear associated with the MJO can alter the vertical structure and tilt of Kelvin waves. Changes in a Kelvin wave's vertical

structure can lead to nonlinear advection of the zonal wind by the vertical wind, leading to accelerations on the timescale of the MJO.

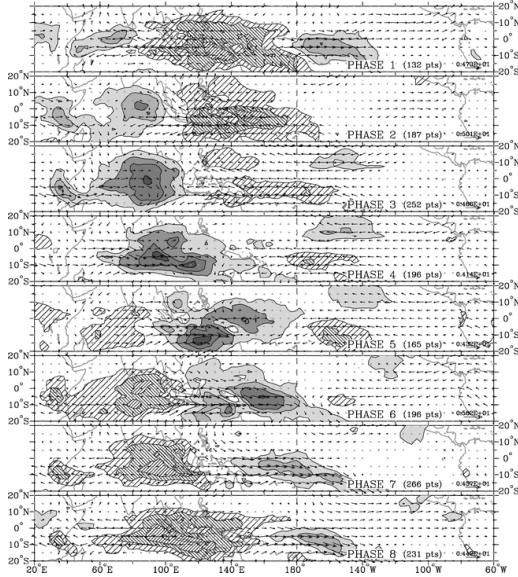


Figure 1: Composite OLR (shaded) and 850 *mb* wind vector anomalies for 8 RMM phases. Solid shading denotes positive OLR anomalies, while hatching denotes negative OLR anomalies. Figure from [5].

1.2 Statement of the Problem

My current research looks at the changes in vertical advection of momentum, heat, and moisture as a Kelvin wave propagates through different phases of the MJO. To expand my understanding of the evolution of Kelvin wave advection in the tropics, this study looks at a different aspect of the state equation: the vertical turbulent flux of momentum, heat, and moisture. Explicitly, I calculated the vertical turbulent flux of momentum, heat, and moisture in the tropics as a Kelvin wave propagates from 60°*E* to 120°*E* during the eight phases of the MJO. I chose this region to compare the effects of Kelvin waves and the MJO to turbulent flux over the Indian ocean versus the Maritime Continent.

1.3 Research Questions

- How does the vertical structure of the turbulent fluxes change over water (Indian ocean) versus over land (Maritime Continent)?
- How do the turbulent fluxes behave during the enhanced convective phase versus the suppressed convective phase of the MJO?

2 Data and Methods

2.1 Datasets

This study uses gridded data of daily mean OLR from the NCEP Reanalysis data provided by NOAA/OAR/ESRL PSL with a resolution of $2.5^\circ \times 2.5^\circ$ [8]. Outgoing long-wave radiation was used as a proxy for observing convection caused by equatorial waves (following methods in [9]). This study also uses gridded data of air temperature, specific humidity, and zonal and vertical winds from ERA5 provided by ECMWF with a resolution of $1^\circ \times 1^\circ$ from 1000 – 800 hPa. Lastly, this study uses the daily RMM phase data from the International Research Institution (IRI) Climate Data Library in

<https://iridl.ldeo.columbia.edu/>, adapted from [5]. All data spans from January 1979 to December 2020.

The remaining methods use the anomalies of OLR, winds, temperature, and specific humidity with the seasonal cycle removed. To get their anomalies, this study followed the methods prescribed by [10], which uses a simple linear regression model $\mathbf{Y} = \mathbf{X}\mathbf{C} + \epsilon$. Here, \mathbf{X} denotes the predictor matrix, \mathbf{C} denotes the regression coefficients, \mathbf{Y} denotes the observed data, and ϵ denotes the anomalies. Assuming the seasonal cycle follows peaks and troughs, \mathbf{X} contains a column of ones, and three harmonics of sine and cosine waves. The following equation solves for \mathbf{C} .

$$\mathbf{C} = (\mathbf{X}^T \mathbf{X})^{-1} \mathbf{X}^T \mathbf{Y} \quad (1)$$

Thus, $\mathbf{X}\mathbf{C}$ denotes the seasonal cycle, and the anomalies are given by $\epsilon = \mathbf{Y} - \mathbf{X}\mathbf{C}$.

2.2 Fourier Filtering Kelvin wave signals using OLR

This study applied 2-dimensional Fourier transform to OLR anomalies to obtain signals in a wavenumber-frequency spectrum, which closely follows methods from [9] and [10]. The OLR anomalies averaged from latitudes -15° to 15° were arranged into longitude-time arrays. Each longitude-time array was then separated into 96-day segments, and overlapped with its neighbour segments by 48 days to establish smoother tapering. The 2-dimensional Fourier transform of the segmented arrays multiplied by their complex conjugates produces their power spectrum. MATLAB's smoothing function smoothed the power spectrum 30 times along space and time to get the background power spectrum. The original power spectrum divided by the background spectrum gives us the normalized spectrum. A t -test at $\alpha = 0.95$ determines the statistically significant signals in the normalized power spectrum, which describes at what wavenumbers and frequencies the detectable equatorial waves operate (illustrated in Fig. 2). Kelvin waves were arbitrarily set to propagate eastward within wavenumbers 2-9 and frequency 0.05-0.33. Following a band-pass filter, all signals in the normalized power spectrum outside of this domain were then set to zero. From here, applying an inverse Fourier transform on the normalized power spectrum filters the Kelvin wave OLR signals. The subsequent methods use these Fourier filtered OLR anomalies.

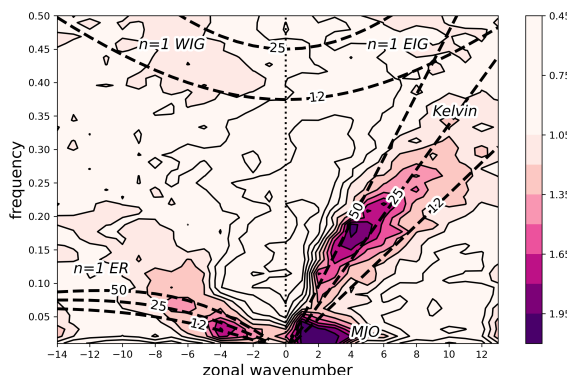


Figure 2: Normalized power spectrum of OLR anomalies (shaded and contoured) after applying 2D Fourier transform. Dispersion curves (dashed lines) show solutions to the shallow water equations from [11] at different equivalent heights (12, 25, 50). Text labels denote equatorial waves.

2.3 Find days with strong Kelvin wave events

This study only considers days with a strong Kelvin wave propagating through the different phases of the MJO while passing through every 5° base longitude from 60°E to 120°E . Strong Kelvin wave events consider all days with (1) negative OLR anomalies at each base longitude that are also (2) local minima (3) below one standard deviation of the whole time series. Days with strong Kelvin waves passing through each base longitude were further separated into each phase of the MJO. In the end, we should get a list of days for each pair of base longitude and phase of the MJO.

2.4 Calculating turbulent fluxes

The equations for mean momentum, heat, and moisture in turbulent flow is given, respectively, by

$$\begin{aligned} \frac{\partial \bar{U}}{\partial t} + \bar{U}_j \frac{\partial \bar{U}}{\partial x_j} &= -f_c (\bar{V}_g - \bar{V}) - \frac{\partial(\bar{u}'_j u')}{\partial x_j} \\ \frac{\partial \bar{\theta}}{\partial t} + \bar{U}_j \frac{\partial \bar{\theta}}{\partial x_j} &= -\frac{1}{\rho C_p} \frac{\partial \bar{Q}_j^*}{\partial x_j} - \frac{L_v E}{\rho C_p} - \frac{\partial(\bar{u}'_j \theta')}{\partial x_j} \\ \frac{\partial \bar{q}_T}{\partial t} + \bar{U}_j \frac{\partial \bar{q}_T}{\partial x_j} &= +S_{qT}/\bar{p}_{\text{air}} - \frac{\partial(\bar{u}'_j q'_T)}{\partial x_j} \end{aligned} \quad (2)$$

In each equation, the first term represents storage, the second term represents advection, the last term represents the turbulent flux divergence, and all other terms represent sundry body forcings. My current research only looks at vertical advection ($j = 3$), but this study looks at the vertical turbulent flux, instead. Explicitly, the vertical turbulent flux of momentum, heat, and moisture, respectively, were calculated following

$$\begin{aligned} \overline{w'w'} \\ \overline{w'\theta'} \\ \overline{w'q'} \end{aligned} \quad (3)$$

Here, the primed variables denote their anomalies previously calculated via regression. The turbulent fluxes from 1000 hPa to 800 hPa were calculated and averaged for the list of days corresponding to each pair of base longitude and MJO phase. For brevity, this paper focuses on comparing the turbulent fluxes at base longitudes 75°E (over the Indian ocean) and 115°E (over the Maritime Continent, but conclusions apply for all base longitudes. All plots for the other base longitudes are in the Appendix.

3 Results and Discussion

3.1 Turbulent vertical momentum flux

The turbulent vertical momentum flux along each base longitude and at different phases of the MJO are shown in Fig. 3. The solid dashed line denotes the average across all MJO phases at that base longitude. Generally, the momentum flux tends to be more positive over water than land. Over the Maritime Continent, the momentum flux doesn't change much within the boundary layer across the different MJO phases. An inversion in the vertical structure also becomes apparent at around 850 m altitude over the Maritime COntinent, something absent over the Indian ocean. Generally the momentum flux tends to be more positive during RMM 1 and 6 over water, the suppressed convective phase of the MJO in that region. On the other hand, the momentum flux tends to be more positive over land during RMM 2, 3, and 4, the enhanced convective phase of the MJO in that region.

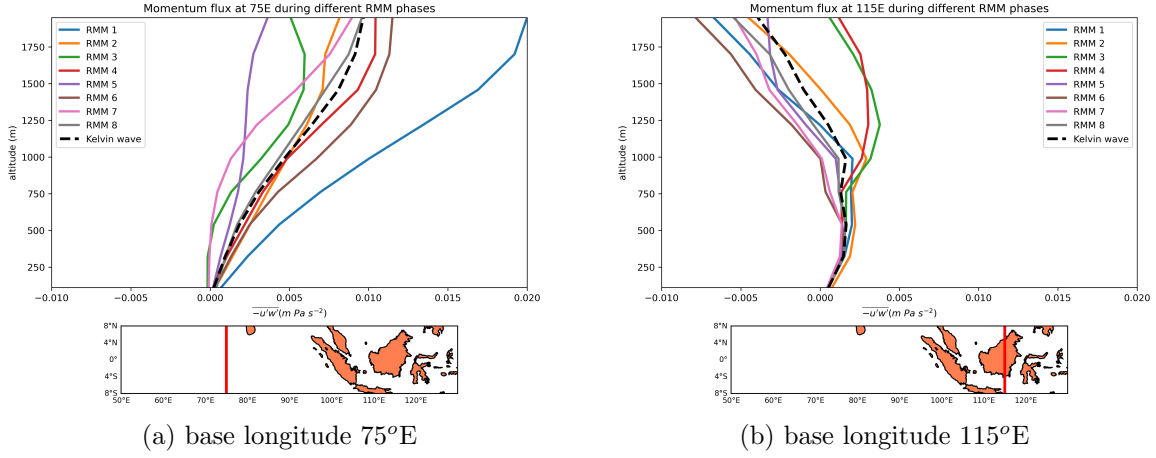


Figure 3: Vertical turbulent momentum flux during RMM phase 1 to 8 at base longitudes (a) 75°E and (b) 115°E . The black dashed line denotes the average momentum flux across all RMM phases.

3.2 Turbulent vertical heat flux

The turbulent vertical heat flux along each base longitude and at different phases of the MJO are shown in Fig. 4. Within the boundary layer the heat flux increases with height, while it decreases with height at higher altitudes. The vertical structure of the heat flux tends to invert around 1000 over water and around 600 m over land.

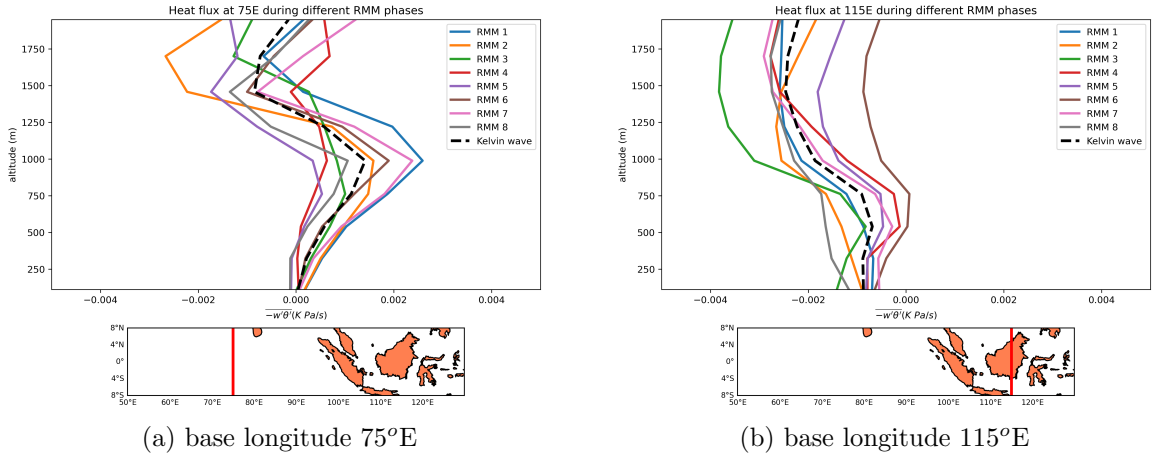


Figure 4: Same as Fig. 3 but for heat flux.

Unlike the momentum flux, the effects of the changes in the MJO phase on the heat flux at the boundary layer becomes more apparent over land than over water. However, looking closely, the heat flux tends to be more positive during RMM 1, 6, and 7 over water, the suppressed convective phase of the MJO in that region. On the other hand, the heat flux tends to be more positive during RMM 4, 5, and 6 over land, the enhanced convective phase of the MJO in that region.

3.3 Turbulent vertical moisture flux

The turbulent vertical moisture flux along each base longitude and at different phases of the MJO are shown in Fig. 5. Looking at their vertical structures, the moisture flux

increases more rapidly with height over water than over land. Over the Maritime Continent, the moisture flux decreases with height until reaching around 500 m where it begins to increase with height as well.

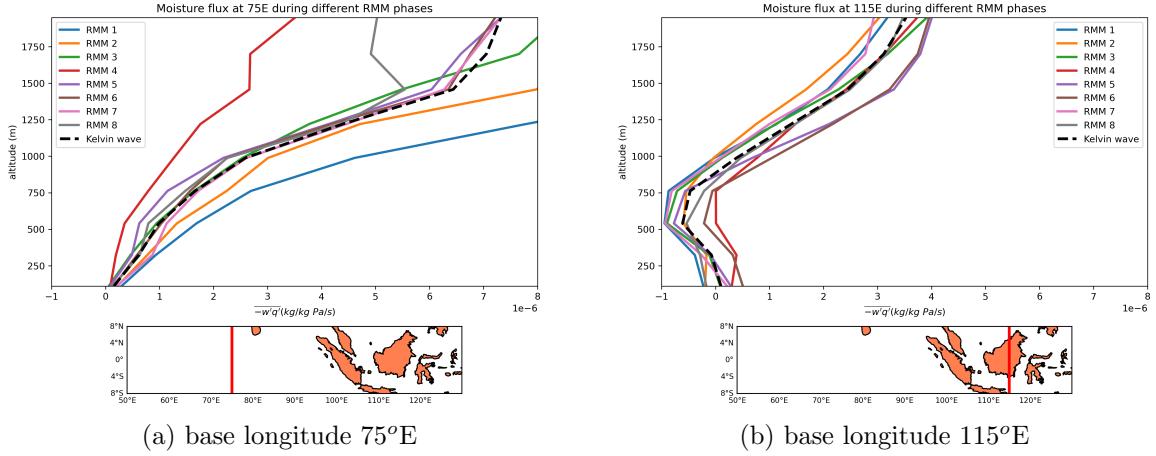


Figure 5: Same as Fig. 3 but for moisture flux.

Similar to the momentum flux, the effect of changes in the phases of the MJO are more evident over water than over land. Looking more closely, the moisture flux increases with height the fastest during RMM 1, 2, and 8 over water, the suppressed convective phase of the MJO in that region.

4 Summary and Conclusions

This study obtained the days with strong Kelvin waves passing through different base longitudes during different phases of the MJO. The vertical turbulent flux of momentum, heat, and moisture were then calculated during each Kelvin wave event.

Momentum flux tends to be more positive over water than land, and the effects of the MJO on the boundary layer becomes more evident over water than land. On the other hand, the heat flux tends to be more positive during the MJO's suppressed convective phase over water, and during the enhanced convective phase over land. The inversion in vertical structure of the heat flux also occurs at a higher altitude over water than land. Lastly, the moisture flux tends to increase faster with height during the enhanced convective phase of the MJO over water. The moisture flux also rapidly increases with height over water, but inverts first in vertical structure at around 500 m over land.

References

- [1] G. N. Kiladis, M. C. Wheeler, P. T. Haertel, K. H. Straub, and P. E. Roundy, Convectively coupled equatorial waves, *Reviews of Geophysics* **47** (2009).
- [2] J. M. Wallace and V. E. Kousky, Observational evidence of kelvin waves in the tropical stratosphere, *Journal of Atmospheric Sciences* **25**, 900 (1968).
- [3] T. Nakazawa, Tropical super clusters within intraseasonal variations over the western pacific, *Journal of the Meteorological Society of Japan. Ser. II* **66**, 823 (1988).
- [4] R. A. Madden and P. R. Julian, Observations of the 40–50-day tropical oscillation—a review, *Monthly Weather Review* **122**, 814 (1994).
- [5] M. C. Wheeler and H. H. Hendon, An All-Season Real-Time Multivariate MJO Index: Development of an Index for Monitoring and Prediction, *Monthly Weather Review* **132**, 1917 (2004).
- [6] C. J. Schreck, L. Shi, J. P. Kossin, and J. J. Bates, Identifying the MJO, Equatorial Waves, and Their Impacts Using 32 Years of HIRS Upper-Tropospheric Water Vapor, *Journal of Climate* **26**, 1418 (2013).
- [7] K. H. Straub and G. N. Kiladis, The Observed Structure of Convectively Coupled Kelvin Waves: Comparison with Simple Models of Coupled Wave Instability, *Journal of the Atmospheric Sciences* **60**, 1655 (2003).
- [8] E. Kalnay, M. Kanamitsu, R. Kistler, W. Collins, D. Deaven, L. Gandin, M. Iredell, S. Saha, G. White, J. Woollen, et al., The NCEP/NCAR 40-Year Reanalysis Project, *Bulletin of the American Meteorological Society* **77**, 437 (1996).
- [9] M. Wheeler and G. N. Kiladis, Convectively coupled equatorial waves: Analysis of clouds and temperature in the wavenumber–frequency domain, *Journal of the Atmospheric Sciences* **56**, 374 (1999).
- [10] P. E. Roundy, Interpretation of the spectrum of eastward-moving tropical convective anomalies, *Quarterly Journal of the Royal Meteorological Society* **146**, 795 (2020).
- [11] T. Matsuno, Quasi-geostrophic motions in the equatorial area, *Journal of the Meteorological Society of Japan. Ser. II* **44**, 25 (1966).

Appendix

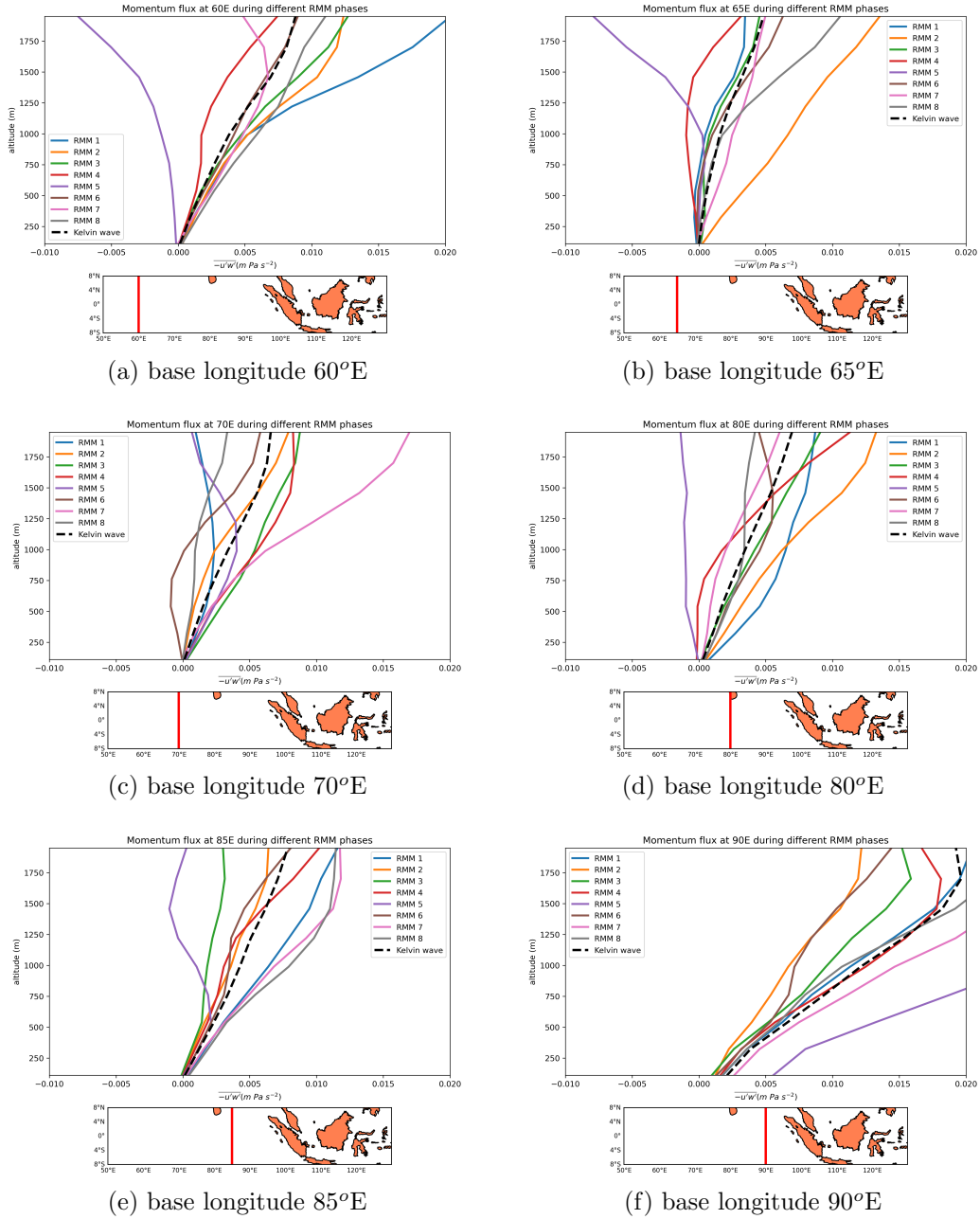


Figure 6: Same as Fig. 3 but for other base longitudes every 5° from 60°E to 115°E

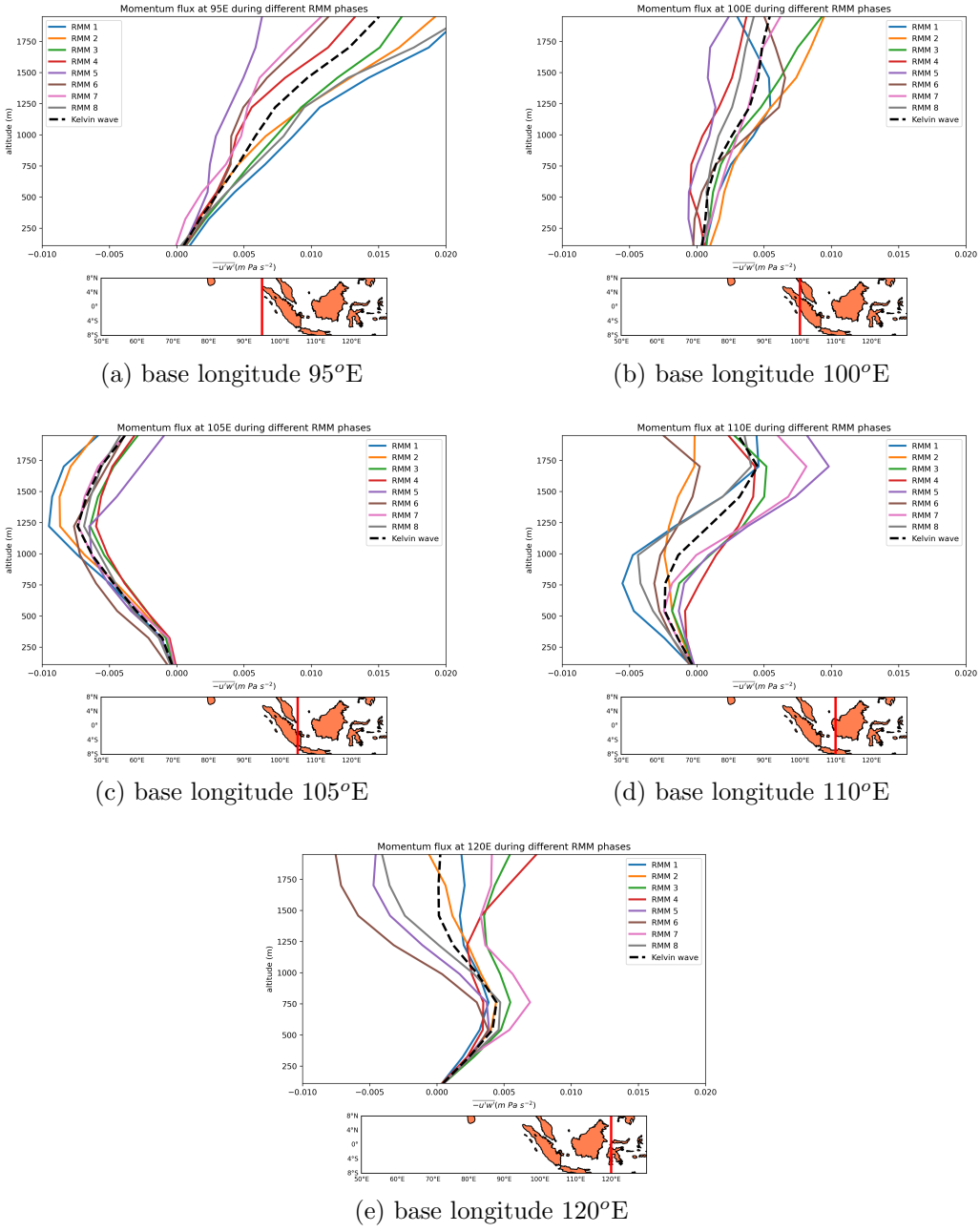


Figure 7: Continuation of Fig. 6

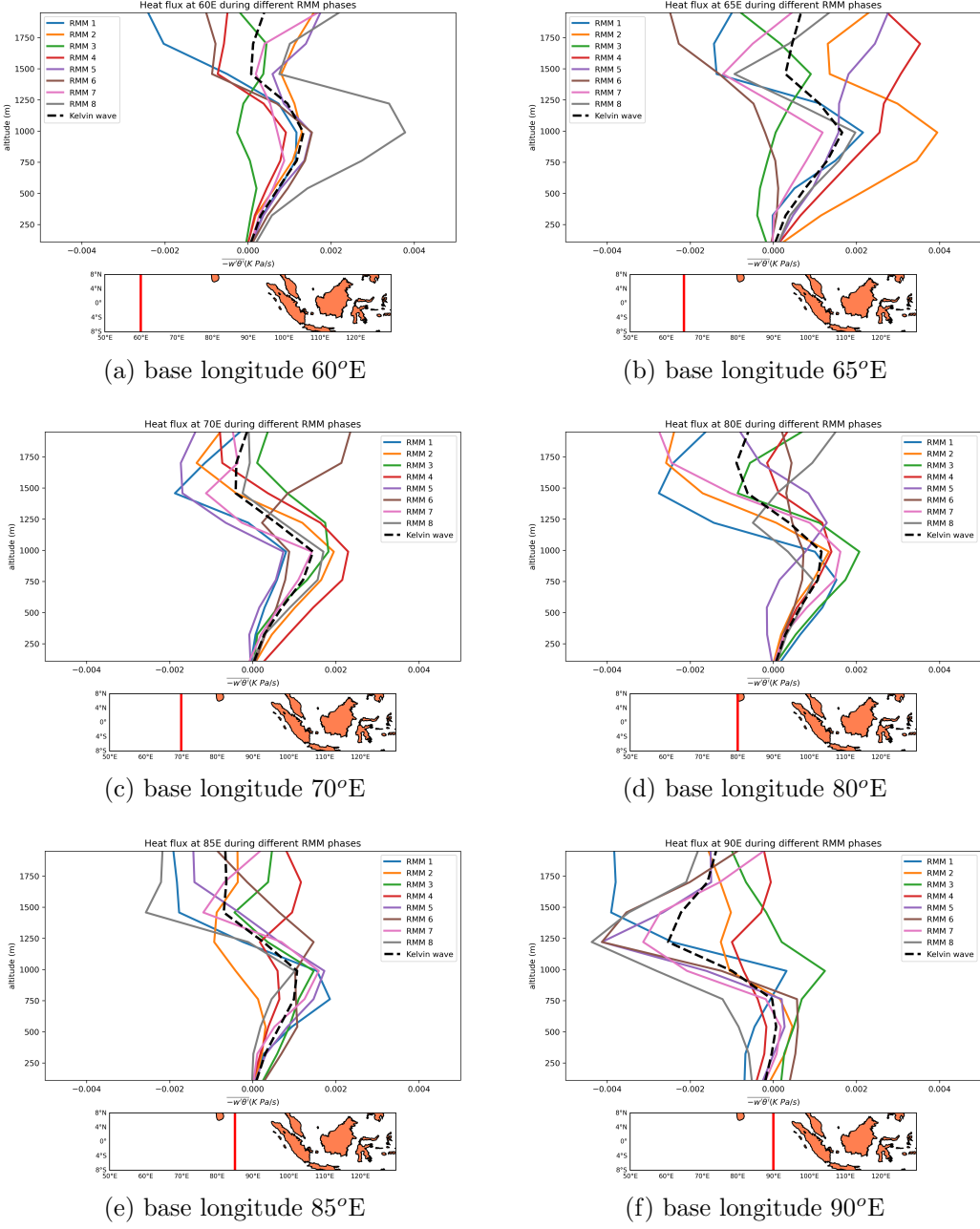


Figure 8: Same as Fig. 4 but for other base longitudes every 5° from 60°E to 115°E

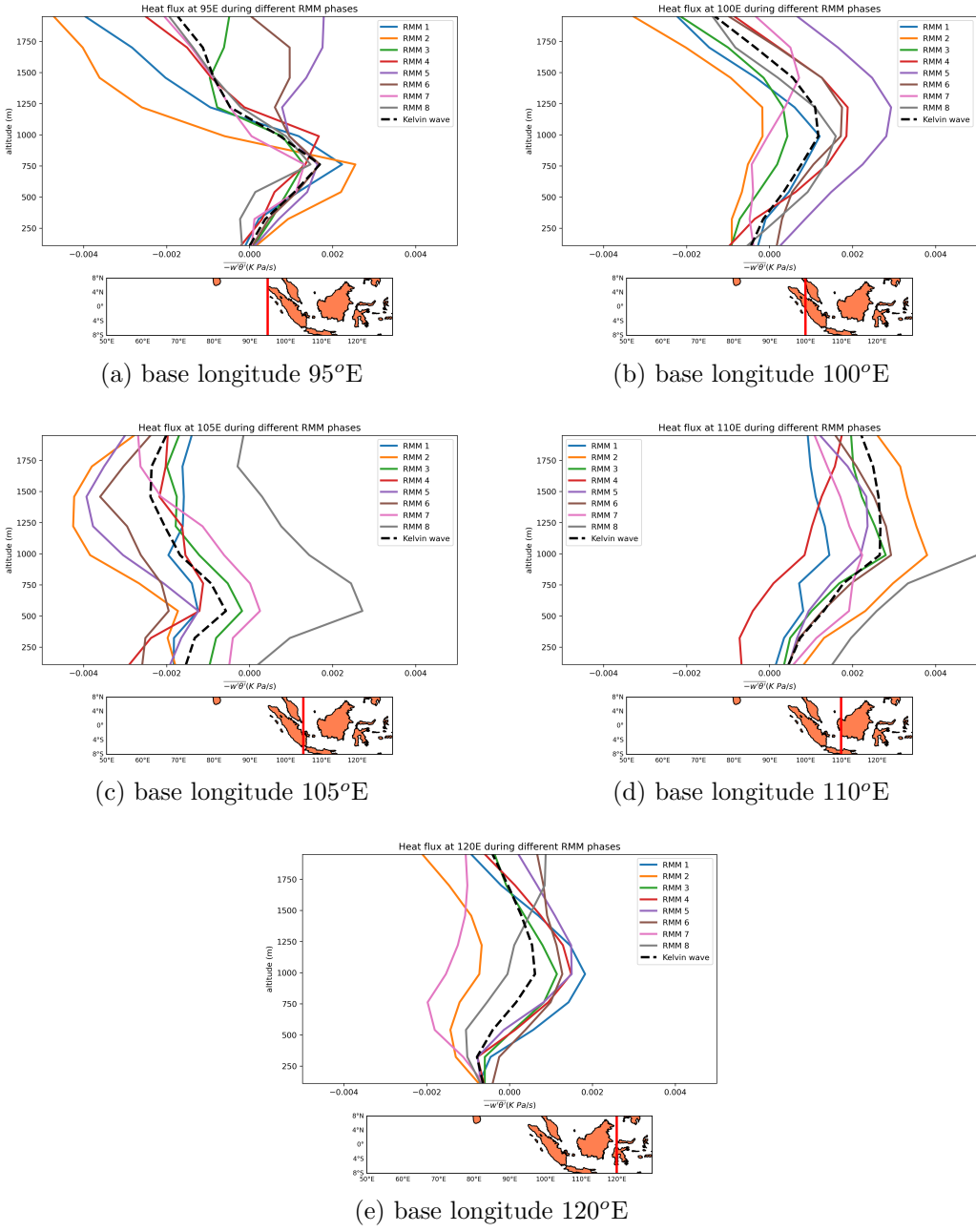


Figure 9: Continuation of Fig. 8

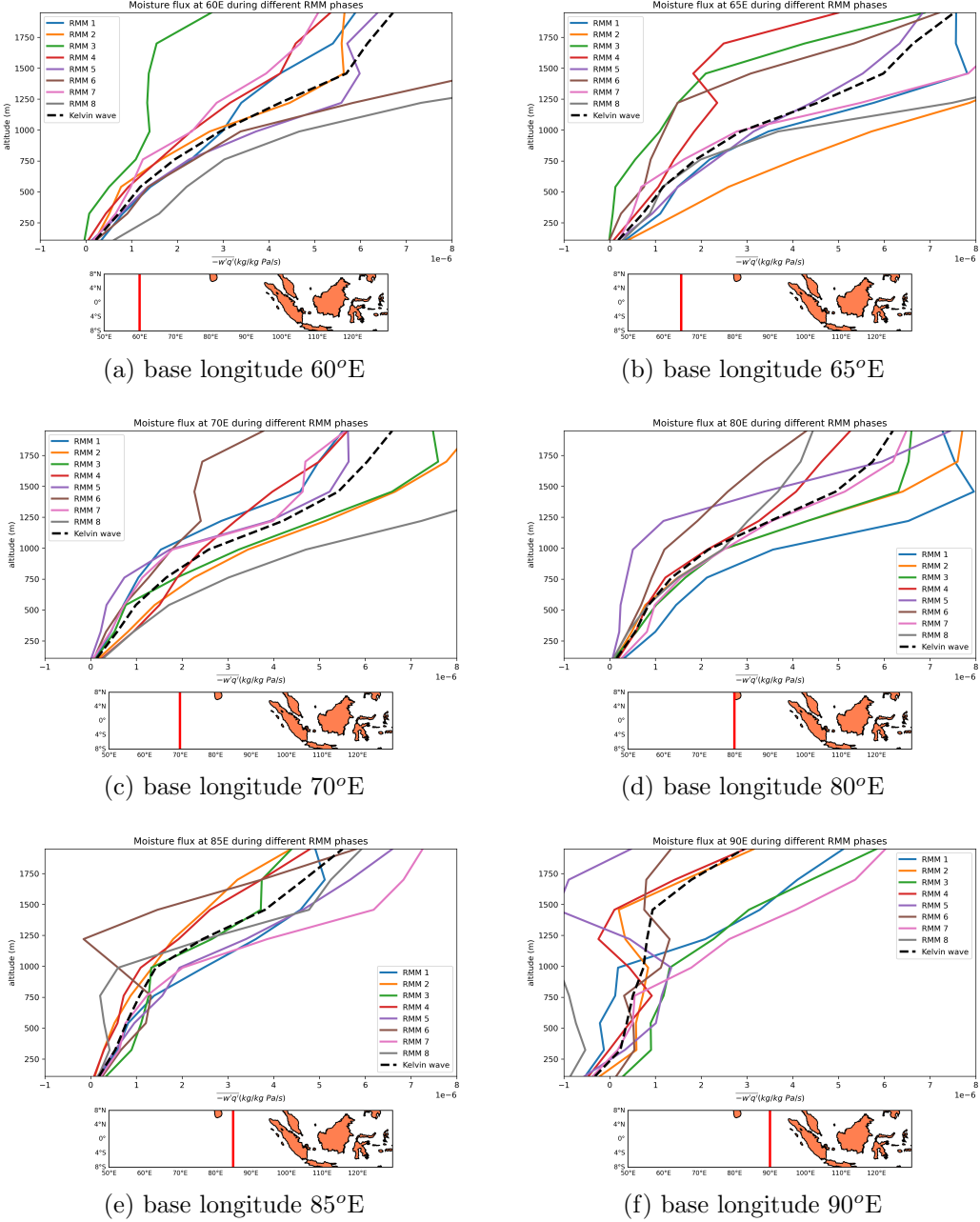


Figure 10: Same as Fig. 5 but for other base longitudes every 5° from 60°E to 115°E

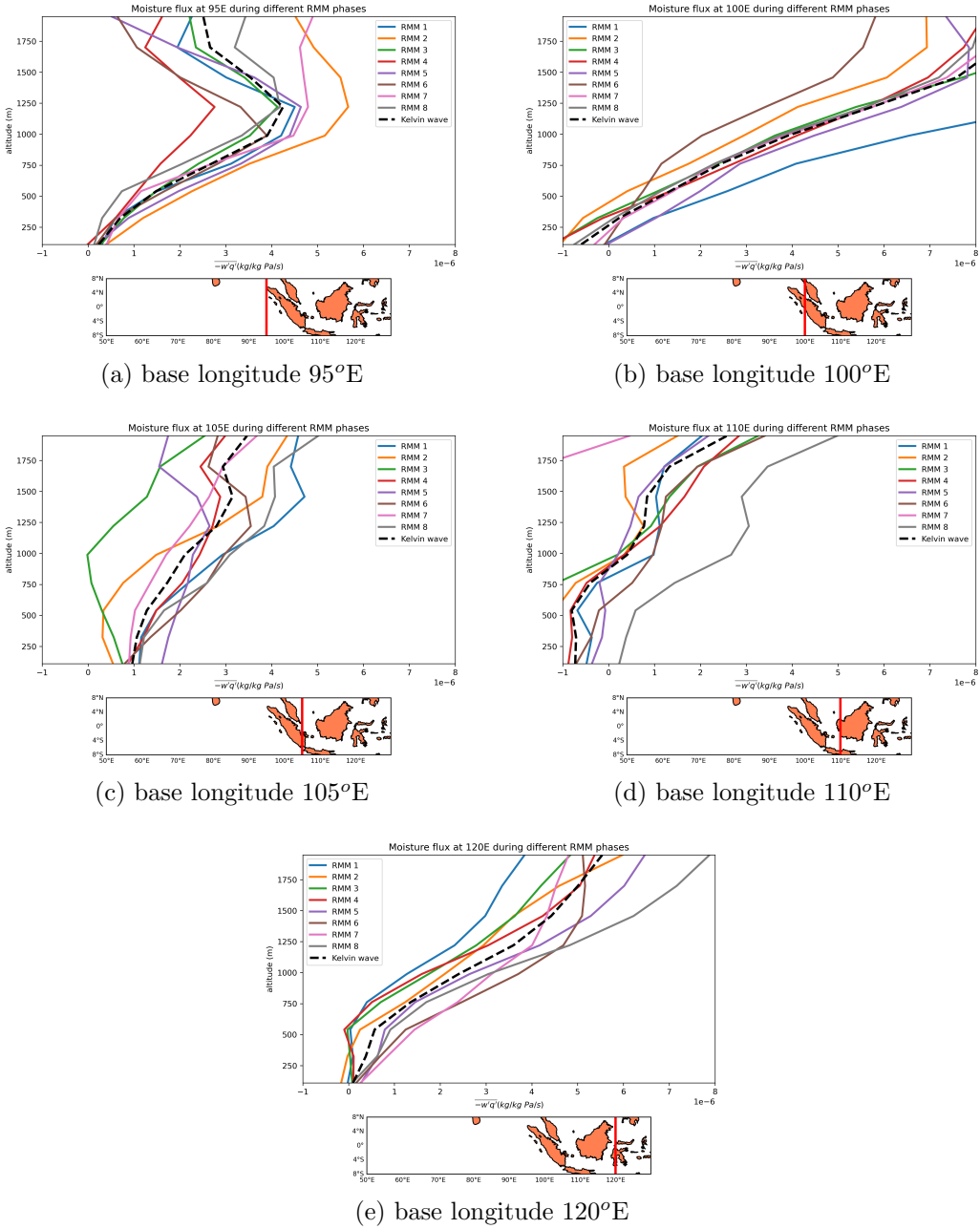


Figure 11: Continuation of Fig. 10